

Efficient Hole Transfer from Monolayer WS₂ to Ultrathin Amorphous Black Phosphorus

Matthew Z. Bellus,[†] Zhibin Yang,[‡] Jianhua Hao,[‡] Shu Ping Lau,[‡] and Hui Zhao^{*,†}

[†]*Department of Physics and Astronomy, The University of Kansas, Lawrence, Kansas 66045, United States*

[‡]*Department of Applied Physics, The Hong Kong Polytechnic University, Hung Hom Kowloon, Hong Kong, Peoples Republic of China*

E-mail: huizhao@ku.edu

Abstract

The newly developed van der Waals materials allow fabrication of multilayer heterostructures. Early efforts have mostly focused on heterostructures formed by similar materials. More recently, however, attempts have been made to broadening the types of materials, such as topological insulators and organic semiconductors. Here we introduce an amorphous semiconductor to the material library for constructing van der Waals heterostructures. Samples composed of 2-nm amorphous black phosphorus synthesized by pulsed laser deposition and monolayer WS₂ obtained by mechanical exfoliation were fabricated by dry transfer. Photoluminescence measurements revealed that photocarriers excited in WS₂ of the heterostructure transfer to amorphous black phosphorus, in the form of either energy or charge transfer, on a time scale shorter than the exciton lifetime in WS₂. Transient absorption measurements further indicate that holes can efficiently transfer from WS₂ to amorphous black phosphorus. However,

interlayer electron transfer of either direction was found to be absent. The lack of electrons transfer from amorphous black phosphorus to WS_2 is attributed to the localized electronic states in the amorphous semiconductor. Furthermore, we show that a bilayer hBN can effectively change the hole transfer process, with allowed observation of trions due to charge imbalance. These results establish amorphous black phosphorus as a building block for van der Waals heterostructures, provide new information for understanding interlayer charge transfer, and allow connection of amorphous materials by van der Waals interfaces.

KEYWORDS: two-dimensional material, amorphous semiconductor, transition metal dichalcogenide, charge transfer, transient absorption

Recently, two-dimensional (2D) materials have drawn considerable attention for both fundamental research and applications due to their novel electronic and optical properties.¹⁻⁵ One of the intriguing aspects of these materials is that they can form multilayer heterostructures *via* van der Waals interlayer interaction.⁶ Unlike ionic and covalence bonds, van der Waals interaction does not have atomic-level correspondence. This is a significant advantage over traditional heterostructure that can only be formed by materials with similar lattice structures. Since lattice match is no longer a constrain, a large number of materials can be chosen from to assemble multilayers with certain properties. Hence, this new approach can produce a vast number of new materials for many applications, and can potentially transform material discovery.^{7,8} The interfaces in such structures are atomically sharp and the junctions can be as thin as two atomic layers - both reaching the ultimate limits.

Since 2013, the study of van der Waals heterostructures has gained significant momentum. The majority of the efforts have been devoted to heterobilayers formed by transition metal dichalcogenide (TMD) and graphene or by two types of TMDs, respectively. Combining graphene with TMD is beneficial for optoelectronic applications,^{9,9-12} since the former can serve as electrodes¹³ while the latter, the light absorption or emission layer.¹⁴ Study of

TMD-TMD heterobilayers can provide valuable information on van der Waals interlayer coupling, and achieve tuning of the optical and transport properties of these materials.^{15–23} In these van der Waals heterostructures, the two materials have similar lattice structures. Layer-coupled states can form, which can help integration of electronic and optical responses of the two layers. For example, layer-coupled states could be responsible for the observed ultrafast interlayer charge transfer in TMD-TMD heterobilayers.

The removal of lattice-matching requirement invites inclusion of materials with different lattice properties to form heterostructures. In principle, combining 2D materials with different lattice structures (and thus likely different properties) can produce heterostructures with widely tunable properties. Demonstration of high-performance van der Waals heterostructures of materials with significantly different lattices structures will expand the material library and vastly increase the possible material combinations. Very recently, a number of 2D materials with different lattice structures have been used to successfully form heterostructures with TMD and graphene, including phosphorene,^{24–26} GaTe²⁷ Bi₂Se₂,²⁸ CrI₃,²⁹ and even organic materials^{30–34}

Here we introduce a noncrystalline semiconductor, namely amorphous black phosphorus (aBP), to the 2D heterostructure library. Amorphous semiconductors are of great importance in the electronics industry. They are an interesting class of materials, as their amorphous structure omits one of the most fundamental characteristics utilized in solid state physics, crystallinity. The lack of long-range periodicity often leads to very fuzzy electronic states and poor electronic performance compared to their crystalline counterparts. However, low fabrication costs makes these types of materials highly desirable for applications that do not require superior performance. Most notably, amorphous silicon has been widely used for common photovoltaic devices³⁵ and thin-film transistors.³⁶ Amorphous In-Ga-Zn-O has shown promise for transparent thin-film transistors with reported mobilities exceeding 10 cm² V⁻¹ s⁻¹.³⁷ Additionally, amorphous SiO₂ is widely used as a gate dielectric in the electronics industry. Amorphous materials have also been used as reaction catalysts, with

amorphous iron being used to aid in the hydrogenation of carbon monoxide,³⁸ and amorphous metal-oxides as an oxygen evolution reaction catalyst.³⁹

In this work, we fabricate heterostructures of monolayer WS_2 and 2-nm aBP, and study their charge carrier dynamics. Recently, ultrathin films of aBP have been successfully synthesized by some of us, with other collaborators.⁴⁰ We found that in WS_2 /aBP heterostructures, holes excited in WS_2 transfer to aBP on an ultrafast time scale. Electrons, on the other hand, do not transfer, neither from WS_2 to aBP nor the opposite direction. The charge transfer results in extended lifetime of photoexcited electrons in WS_2 . We also show that a bilayer hBN can slow down the hole transfer and lead to observation of trions in WS_2 . These results introduce amorphous semiconductors to the library of building blocks for van der Waals heterostructures, provide new ingredient for understanding the mechanisms of interlayer charge transfer, and offer a method to make connections to amorphous materials through other 2D crystalline materials.

Results and Discussion

Sample and Photoluminescence

Figure 1(a) shows an optical microscope image of the sample studied. A uniform 2-nm aBP layer was deposited on a Si/SiO₂ substrate (see Methods), as shown as the pinkish colored background. To study effects of potential charge transfer between WS_2 and aBP, we first transferred a thick hBN flake on aBP (outlined by the white line). It contains more than 15 layers. We then transferred a monolayer (ML) WS_2 (outlined by blue) near the edge of the hBN flake. The region directly on aBP forms the heterostructure sample, while that on hBN serve as a ML WS_2 individual layer for comparison, since the thick hBN layer is expected to block the interactions between WS_2 and aBP effectively.

From first-principle calculations, the electron affinity and the ionization potential of ML WS_2 are -3.8 and -5.9 eV, respectively,⁴¹ as schematically shown in Figure 1(b). Based

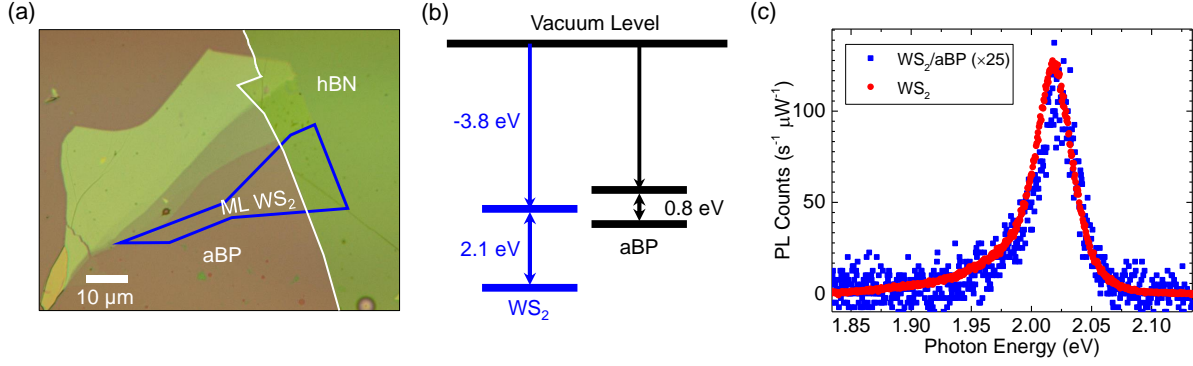


Figure 1: (a) Optical microscope images of the WS_2/aBP sample. ML WS_2 is outlined by blue and hBN by white. Part of WS_2 is directly on top of aBP, while the rest is on hBN flake. (b) The expected band alignment of ML WS_2 and aBP. (c) Photoluminescence spectra of ML WS_2 directly on aBP (blue squares, multiplied by 25) and on hBN (referred to as WS_2 , red circles).

on previous measurements, the optical bandgap of 2-nm aBP is about 0.8 eV.⁴⁰ However, information on the electron affinity and ionization potential of aBP is still missing. To speculate the nature of the band alignment of the WS_2 -aBP heterostructure, one could use the values of crystalline BP as a reference. The bandstructure of crystalline BP is highly sensitive to thickness. Hence, one should use the values that best represent the 2-nm thick aBP, which correlates to about 3 layers. The calculated electron affinity of trilayer BP is about -4 eV.^{42?} Using the 2-nm bandgap of aBP of 0.8 eV, a ionization potential of -4.8 eV could be inferred. Given that this value is more than 1 eV from that of WS_2 , it appears to be safe to assume that the valence band maximum (VBM) of aBP is above WS_2 . However, since the electron affinity of the two materials are similar, the band alignment of WS_2/aBP could be either type-II, as indicated in Figure 1(b), or type-I with the conduction band maximum (CBM) of aBP below that of WS_2 . In the following discussions, we will present evidence that the alignment is indeed type-II.

The sample was characterized by using photoluminescence (PL) spectroscopy. A continuous-wave 405-nm laser was focused through a $100\times$ objective lens on to the sample. When the laser spot was placed on the WS_2 region on hBN, a strong PL peak at about 2.02 eV was

observed (red circles). The PL yield, peak energy, and the lineshape are all consistent with previous reports.^{43–46} This confirms the ML thickness of the WS₂ and the effectiveness of the thick hBN layer of separating WS₂ and aBP. In the rest discussions, we will refer this region of the sample as ML WS₂. With the laser spot move to the region of WS₂ that is directly on top of aBP, there is significant quenching of the PL, by about a factor of 25 (blue squares). This quenching indicates that charge or energy transfer occurred from WS₂ to aBP. Without such transfer, excitons would be expected to stay in WS₂ and recombine, contributing to the PL signal. The large quenching factor suggests that such transfer occurs on a time scale that is much shorter than the exciton lifetime in an individual WS₂ ML.

Ultrafast hole transfer from WS₂ to aBP

The PL quenching of WS₂ by aBP can originate from charge transfer or energy transfer from WS₂ to aBP. In the former case, one type of carriers (likely the holes) transfer to aBP. If the excited electrons reside in WS₂, they cannot recombine with the holes and contribute to PL. In energy transfer, both electrons and holes transfer to aBP, which also results in a reduction of WS₂ PL yield. To resolve the transfer dynamics and probe the physics mechanisms involved, we performed transient absorption measurement in reflection geometry (see Methods).

First, we studied photocarrier dynamics in the ML WS₂ region. Carriers are injected by a 3.2-eV pump pulse with a peak fluence of 0.46 $\mu\text{J cm}^{-2}$. With an absorption coefficient of $0.72 \times 10^6 \text{ m}^{-1}$,¹⁴ this corresponds to an injected areal carrier density of $4.37 \times 10^{10} \text{ cm}^{-2}$. The red circles in Figure 2(a) show the differential reflection signal of a 2.0-eV probe, which is tuned near the A-exciton resonance of ML WS₂. The rise of the signal can be fit by the integral of a Gaussian function with a full width at half maximum of 0.37 ps, as indicated as the solid curve in the inset. Since the width of the pump and probe pulses are both about 0.25 ps at the sample location (due to the chirp introduced by the objective lens), this value is close to the instrumental response time. This suggests that

the pump-injected electron-hole pairs produce a peak differential reflection signal at the A-exciton resonance on a time scale shorter than the instrumental response time, which is consistent with previous reports.^{47–49} The decay of the signal can be fit by an bi-exponential function, $\Delta R/R_0(t) = A_1 \exp(-t/\tau_1) + A_2 \exp(-t/\tau_2) + B$. The black curve over the symbols show that the fit is satisfactory, with parameters of $A_1 = 1.51 \times 10^{-3}$, $A_2 = 1.19 \times 10^{-3}$, $B = 0.08 \times 10^{-3}$, $\tau_1 = 0.59 \pm 0.1$ ps, and $\tau_2 = 13 \pm 1$ ps. The bi-exponential dynamics and these time constants are both reasonably consistent with previous reports on ML WS₂.^{47–49} The short time constant of τ_1 can be attributed to formation of excitons from the injected electron-hole pairs;⁴⁷ while the long time constant τ_2 indicates the lifetime of excitons.^{48,49} To probe the possible contributions from the aBP layer underneath hBN to the signal, we repeated the measurement with the laser spots located at a region not covered by WS₂. The results are shown by the gray triangles in Figure 2. The lack of a detectable signal is expected,⁵⁰ since the probe photon energy is much higher than the bandgap of 0.8 eV of the aBP layer.

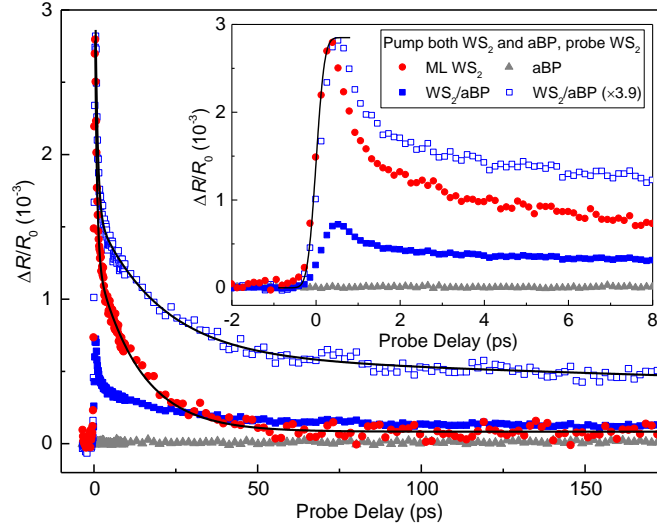


Figure 2: Time-resolved differential reflection measurements with a 3.2-eV pump and a 2.0-eV probe. Solid symbols represent results from different regions of the same sample. Open symbols is scaled for better comparison. The inset provides a closer look of the data near zero probe delay.

We next repeated the measurement by moving the laser spots to the region of WS₂/aBP.

Without interlayer transfer, one would expect a similar signal since the same density of carriers are be injected in WS₂ and will produce a signal with the same time evolution, while carriers injected in aBP will not contribute to the signal. However, as shown by the blue solid squares in Figure 2(a), we observed a signal that is a few times smaller and decays at a slower rate. To better compare this signal with that from the ML WS₂ region, the signal is multiplied by 3.9, as shown by the blue open squares. Clearly, the majority of the signal decays slower than ML WS₂. The significant differences in both the magnitude and the dynamics of the two signals strongly suggest that there is substantial interlayer transfer from WS₂ to aBP: If WS₂ and aBP are non-interacting individual materials, the signal from the heterostructure should be similar to that of WS₂ ML.

Close examination of the signal from the heterostructure revealed that the scaled signal can be fit by a tri-exponential function, $\Delta R/R_0(t) = A_1 \exp(-t/\tau_1) + A_2 \exp(-t/\tau_2) + A_3 \exp(-t/\tau_3)$ (black curve), with parameters of A_1, A_2 , and A_3 of 2.4, 1.0, and 0.6×10^{-3} , and τ_1, τ_2 , and τ_3 of 0.7 ± 0.1 , 19.6 ± 2 , and 697 ± 150 ps. The sub-ps component contributes to about 60 % of the total signal, which is similar to the ML WS₂ data. It can be attributed to the same origin of exciton formation. the other two time constants show that the carrier lifetime in WS₂ is significantly extended in the heterostructure.

The possible candidates for interlayer transfer include energy transfer and charge transfer. The energy transfer can be achieved by either Fröster mechanism,⁵¹ where elimination of one exciton in WS₂ induces an exciton or electron-hole pair in aBP, or Dexter mechanism,^{52,53} where an exciton moves from WS₂ to aBP. In both cases, however, the decay of the signal should be faster than ML WS₂ since the energy transfer provides an additional channel for reducing the carrier density in WS₂. This contradicts to the data. On the other hand, charge transfer (either electrons or holes) from WS₂ to aBP would leave one type of carriers in WS₂, causing a smaller but long-living signal since their recombination will be suppressed by charge separation. Both these features are consistent with the data. Given the large valence band offset between WS₂ and crystalline BP [Figure 1(b)], we expect the transferred

carriers to be the holes.

Based on this interpretation and the pronounced PL quenching shown in Figure 1(c), the hole transfer from WS_2 to aBP occurs on a time scale much shorter than the exciton lifetime in ML WS_2 . The reduced differential reflection signal of the heterostructure in comparison to WS_2 suggests that the transfer occurs on a time scale comparable to or much shorter than the pulse width of about 0.3 ps. Otherwise, the initial peak of the signal should be similar between the two regions, and there would be an additional decay component that is shorter than 13 ps. Once the holes transferred, the electrons reside in WS_2 and are separated from holes, and thus have an extended lifetime of about 700 ps. The extended carrier lifetime due to charge separation is consistent with previous observations in various type-II van der Waals heterostructures.^{17,18,54–56} Finally, we attribute the τ_2 process to the recombination of excitons in WS_2 , with holes that do not transfer. It was known that interfacial contaminations⁵⁷ can separate the two layers and block interlayer transfer. In the measurement, the region of the sample excited by the laser spots inevitably contains parts with relatively poor interface. Excitons in these regions recombine efficiently due to the lack of charge transfer, producing this WS_2 -like process.

Lack of electrons transfer from aBP to WS_2

The lack of electron transfer from WS_2 to aBP appears to suggest that the CBM of WS_2 is lower than aBP, as plotted in Figure 1(b). As such, it is interesting to study if electrons in aBP can transfer to WS_2 , which is allowed by the band alignment. In the measurement summarized in Figure 2, the aBP layer was also excited. However, since the probe senses carriers in WS_2 and cannot distinguish between electrons and holes, it is difficult to isolate potential contributions from the electrons transferred from aBP.

To better study the potential transfer of electrons from aBP to WS_2 , we performed another set of measurements where only aBP is pumped and probed. Here, a 1.55-eV pump is used to inject carriers in aBP, which are probed by a 0.8-eV pulse that is tuned to its

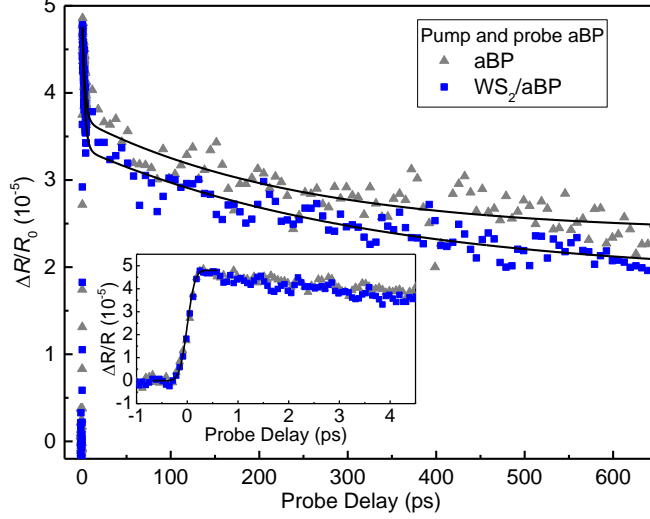


Figure 3: Time-resolved differential reflection measurements with a 1.55-eV pump and a 0.8-eV probe. Solid symbols represent results from different regions of the same sample. Open symbols is scaled for better comparison. The inset provides a closer look of the data near zero probe delay.

bandgap. We first studied the aBP sample. The differential reflection with a pump fluence of about $50 \mu\text{J cm}^{-2}$ is on the order of 5×10^{-5} , as shown by the gray triangles in Figure 3. This is reasonably consistent with our recent measurements on similar samples.⁵⁰ As shown in the inset, the signal raises to a peak quickly. The solid line in the inset is the integral of a Gaussian function with a FWHM of about 0.3 ps. The decay of the signal was fit by an bi-exponential function with a background, $\Delta R/R_0(t) = A_0 + A_1 \exp(-t/\tau_1) + A_2 \exp(-t/\tau_2)$, with the parameters of A_0, A_1, A_2 of 2.4, 1.6, 1.3×10^{-5} , and τ_1, τ_2 of 2.9 ± 0.6 and 244 ± 50 ps, respectively. We can attribute the τ_1 process to thermalization or exciton formation, and τ_2 to photocarrier lifetime in aBP. The background is likely induced by trapping of carriers by defects or thermal effects. The most important finding in this set of measurements is that, the signal obtained from the WS_2/aBP heterostructure region is very similar to aBP, as shown by the blue squares in Figure 3. By fitting the data with the same function, we found that for the heterostructure, A_0, A_1 , and A_2 are 1.9, 1.5, and 1.5×10^{-5} , with τ_1 and τ_2 of 2.7 ± 0.6 and 226 ± 50 ps. This shows that the electrons excited in aBP do not transfer to WS_2 . Otherwise, the signal in the heterostructure would have been lower and it would

have decays slower.

The lack of electron transfer from aBP to WS_2 is interesting. It suggests that although efficient charge transfer can occur from the crystalline to amorphous layer, the opposite transfer is inefficient. This can be attributed to the amorphous nature of aBP: due to the lack of a long-range lattice, electron states in aBP are expected to be largely localized. The localization of the electron wavefunction can prohibit transfer to WS_2 even if there are lower energy states available in WS_2 . It is also possible that aBP does not have a well defined bandedge, and hence there exist conduction band states below WS_2 .

Control of charge transfer and trion formation

Having demonstrated the ultrafast hole transfer from WS_2 to aBP and the lack of electron transfer from aBP to WS_2 , we next explore control of charge transfer by using a thin hBN barrier. We first exfoliated a thin hBN flake onto PDMS and then transferred it to on top of aBP. Figure 4(a) shows the green-channel microscope image of this flake, which clearly shows step-like contrasts with regions of 4.3% and 8.3%, as indicated in the figure. Previously, it has been shown that these contrasts correspond to monolayer and bilayer flakes.^{58,59} We next transferred a WS_2 ML flake partially on the bilayer hBN region. The black triangles in Figure 4(c) show the PL spectrum from part of the WS_2 flake on bilayer hBN under the 405-nm excitation. The main peak is slightly shifted to low-energy side compared to WS_2 /aBP (blue squares). Its peak is about 3 times higher than WS_2 /aBP, and is thus about 8 times lower than WS_2 ML [Figure 4(c)]. This feature shows that the bilayer hBN can slow down the hole transfer from WS_2 to aBP despite of its ultrasmall thickness. However, the quenching factor of 8 compared to WS_2 ML shows that the hole transfer is still rather efficient.

It is interesting to note that a new peak at low energy side of the main WS_2 peak was observed in WS_2 /bilayer-hBN/aBP. To identify its origin, we measured the PL spectra under various excitation powers, as shown in the left panel of Figure 5. In most of these measurements, there are 3 discernible peaks, labeled as X, T, and L. Each spectra was fit by

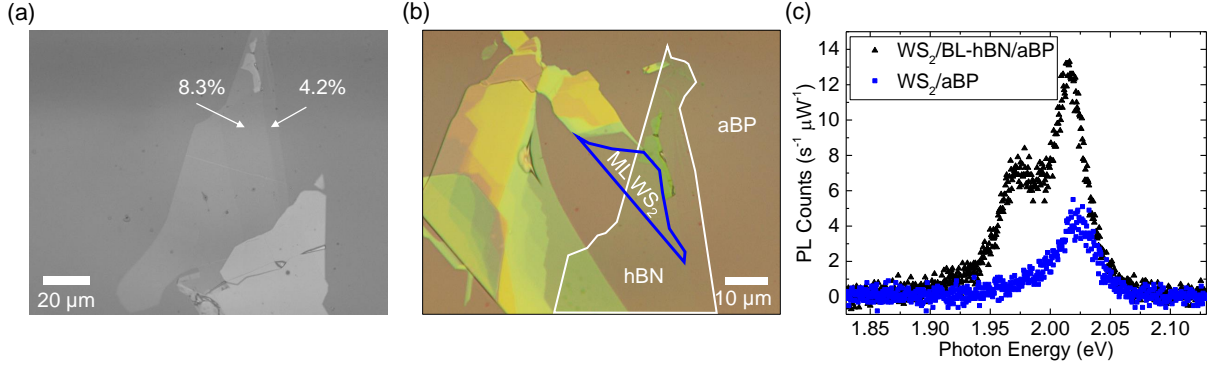


Figure 4: (a) The green-channel image of the hBN flake on aBP before the WS₂ flake was transferred. The regions with contrasts of 4.2% and 8.3% are identified as monolayer and bilayer, respectively. (b) Optical microscope images of the sample after a WS₂ monolayer was transferred partially on aBP and partially on the bilayer region of hBN. (c) Photoluminescence spectra of ML WS₂ directly on aBP (blue symbols) and on bilayer hBN (black).

3 Lorentz peaks except in the lowest-power case, where the L peak was too weak to identify. The blue, red, and purple curves represent the three component peaks, while the yellow curves show the sum. The right panel summarizes the parameters describing these peaks. The X peak has been identified as the A-exciton peak of WS₂, and is almost independent of the excitation power (blue symbols in top panel). The peak shifts to higher energy with excitation power (red symbols in top panel). As a result, the distance between the X and T peaks decrease with power, as shown in the middle panel. This feature suggests that the T peak is from trions in WS₂, with $E_X - E_T$ being the trion binding energy. Extrapolating a rough linear fit back to zero power, we found a zero-density trion binding energy of about 42.5 ± 0.9 meV. This value is consistent with previous reports.^{43,44,60,61} The trend of the peak heights is shown in the lower panel, and in each case it increases fairly linearly, especially in the exciton case (blue). This shows that in this power range, no saturation effects are present. We attribute the appearance of trion PL in this sample to the change of the hole transfer rate by the bilayer hBN, which provides more time for radiative recombination of trions. Furthermore, the more pronounced trion formation in the heterostructure also is also consistent with the lack of electron transfer from WS₂ to aBP, which results in excess

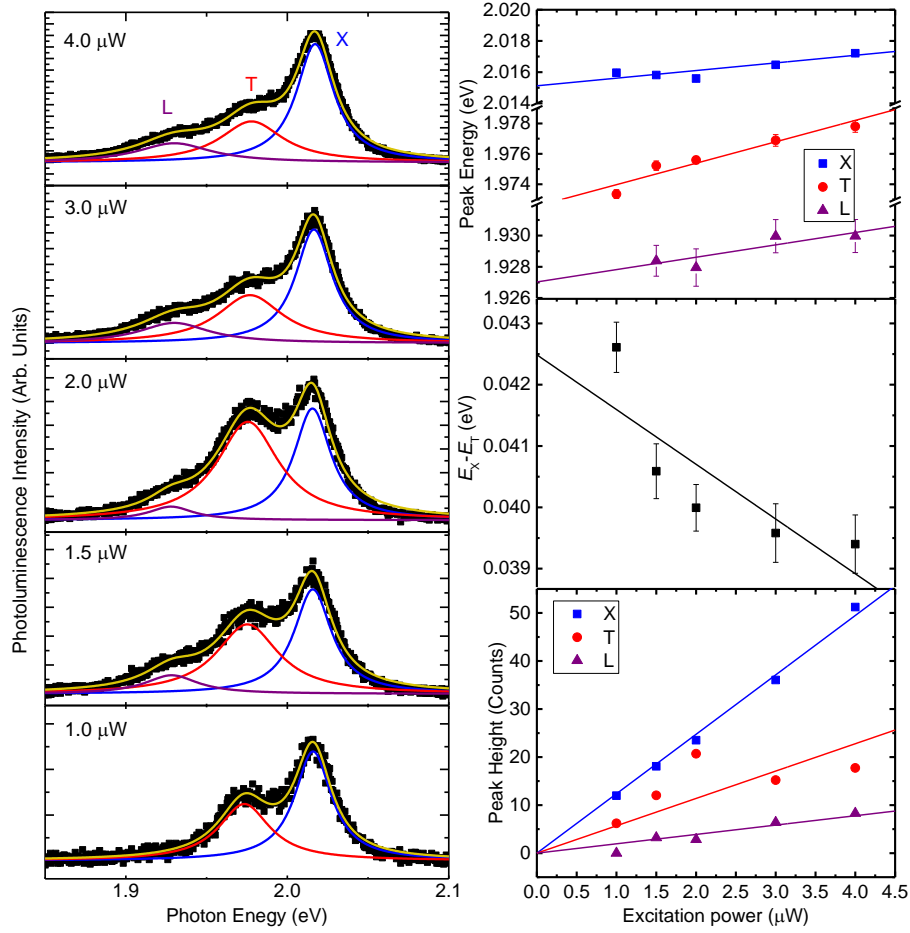


Figure 5: Left panel: Photoluminescence spectra of the $\text{WS}_2/\text{BL-hBN/aBP}$ sample under different 405-nm excitation powers. Each spectrum was fit by three Lorentz peaks (solid lines). Right panels: Peak energy (top), difference of the X and T peak energies (middle), and peak height (bottom) as a function of the excitation power.

electrons in WS_2 during the hole transfer process. This is consistent with the time resolved measurements.

Conclusions

In summary, we have shown that ultrafast and efficient charge transfer can occur between a monolayer crystal and an amorphous semiconducting ultrathin film. We have fabricated heterostructures of monolayer WS_2 and 2-nm amorphous black phosphorus. Significant photoluminescence quenching of WS_2 induced by the amorphous black phosphorus layer indicates efficient excitation transfer from WS_2 to amorphous black phosphorus. The photocarrier dynamics in the heterostructure and the individual component layers of WS_2 and amorphous black phosphorus was studied by transient absorption measurement in reflection geometry. By selectively pumping or probe each layer, we found evidence that holes injected in WS_2 transfer to amorphous black phosphorus on an ultrashort time scale on the order of 100 fs or shorter. On the hand, electrons in neither WS_2 nor amorphous black phosphorus can transfer to the other layer. We attribute the lack of electron transfer from amorphous black phosphorus to WS_2 to the localized nature of electronic states in amorphous materials. Furthermore, we show that a bilayer hBN can effectively change the hole transfer process, with allowed observation of trions due to charge imbalance. These results introduce amorphous black phosphorus as a building block for van der Waals heterostructures, reveal new information for understanding interlayer charge transfer, and provide a method to connect of amorphous materials by van der Waals interfaces.

Methods

Sample Fabrication

Amorphous black phosphorus ultrathin films were synthesized on Si/SiO₂ by pulsed laser deposition. A BP crystal was used as the target. The growth temperature was set at 150°C and the base pressure of the chamber was evacuated to 1.5×10^{-7} Torr. The nominal thickness of the film is 2 nm, according to previously established synthesis conditions.⁴⁰

The heterostructure samples were made by mechanically exfoliating and subsequently transferring monolayer flakes of WS₂ onto the aBP covered substrate. In order to create reasonable control conditions, we first transferred flakes of hBN with varying thicknesses onto regions of the aBP substrates. This is done by mechanically exfoliating flakes of hBN from bulk crystals onto PDMS substrates. The hBN flakes are then transferred onto the aBP covered substrate. Next, monolayer WS₂ flakes were similarly exfoliated onto PDMS substrates and identified by optical contrast. Using the same method as with hBN, they were transferred to the aBP sample, with different regions of the same WS₂ flake overlapping both the hBN layers and the aBP substrate. After the WS₂ was transferred, the samples were annealed for 2 hrs at 75°C in an Ar environment held at a base pressure of 3 torr. This is to help the van der Waals materials adhere better to the aBP. Next, to help preserve the aBP surface from degrading in the ambient conditions of our measurements, the samples were spin coated by a thin layer of PMMA.

Photoluminescence Spectroscopy

The PL spectroscopy measurements were carried out under a 405-nm continuous-wave laser excitation. The laser beam was focused by a microscope objective lens at normal incident. The laser spot is about 1 μm in full width at half maximum, and is located at the central part of a desired sample region. The power of the laser was controlled by a combination of a half-wave plate and a polarizer. The PL from the sample was collected by the same objective

lens and directed into a spectrometer, which is equipped with a thermoelectrically cooled charge-coupled-device camera. To prevent the unwanted light from reaching the detector and affecting the measurement, a set of filters was placed before the spectrometer.

Transient Absorption Measurements

In the transient absorption setup, a Ti-sapphire laser generates 100-fs pulses with a central wavelength tunable from 750 to 850 nm and a repetition rate of 80 MHz. Part of this beam was used to pump an optical parametric oscillator, which outputs a signal pulse tunable from 1100 to 1580 nm. The spectral range can be further extended by second harmonic generation of each output by using a beta barium borate (BBO) crystal. Depending on the measurement, two of these three pulses were used as pump and probe pulses.

In each configuration, the pump and the probe beams were linearly polarized along perpendicular directions. A beamsplitter was used to combine the two beams, which were sent to a microscope objective lens and focused to the sample to spot sizes of 1 - 2 μm in full-width at half-maximum. The reflected probe was collected and collimated by the same objective lens and directed into a biased silicon photodiode, the output of which was measured by a lock-in amplifier that is synchronized with a mechanical chopper that modulates the pump intensity at about 2 KHz. We measured the differential reflection, which is defined as $\Delta R/R_0 = (R - R_0)/R_0$, where R and R_0 are the reflectivities of the probe by the sample with and without the presence of the pump beam, respectively.

Acknowledgments

This material is based upon work supported by the National Science Foundation of USA (DMR-1505852).

References

1. Gibney, E. The Super Materials that Could Trump Graphene. *Nature* **2015**, *522*, 274–276.
2. Neto, A. H. C.; Novoselov, K. New directions in science and technology: two-dimensional crystals. *Rep. Prog. Phys.* **2011**, *74*, 082501.
3. Wang, Q. H.; Kalantar-Zadeh, K.; Kis, A.; Coleman, J. N.; Strano, M. S. Electronics and Optoelectronics of Two-Dimensional Transition Metal Dichalcogenides. *Nat. Nanotechnol.* **2012**, *7*, 699–712.
4. Butler, S. Z.; Hollen, S. M.; Cao, L.; Cui, Y.; Gupta, J. A.; Gutiérrez, H. R.; Heinz, T. F.; Hong, S. S.; Huang, J.; Ismach, A. F. *et al.* Progress, challenges, and opportunities in two-dimensional materials beyond graphene. *ACS Nano* **2013**, *7*, 2898.
5. Lin, Z.; McCreary, A.; Briggs, N.; Subramanian, S.; Zhang, K. H.; Sun, Y. F.; Li, X. F.; Borys, N. J.; Yuan, H. T.; Fullerton-Shirey, S. K. *et al.* 2D Materials Advances: From Large Scale Synthesis and Controlled Heterostructures to Improved Characterization Techniques, Defects and Applications. *2D Mater.* **2016**, *3*, 042001.
6. Geim, A. K.; Grigorieva, I. V. Van der Waals Heterostructures. *Nature* **2013**, *499*, 419–425.
7. Liu, Y.; Weiss, N. O.; Duan, X.; Cheng, H.-C.; Huang, Y.; Duan, X. van der Waals Heterostructures and Devices. *Nat. Rev. Mater.* **2016**, *1*, 16042.
8. Novoselov, K. S.; Mishchenko, A.; Carvalho, A.; Neto, A. H. C. 2D Materials and van der Waals Heterostructures. *Science* **2016**, *353*, 461.
9. Yu, W. J.; Liu, Y.; Zhou, H.; Yin, A.; Li, Z.; Huang, Y.; Duan, X. Highly Efficient Gate-Tunable Photocurrent Generation in Vertical Heterostructures of Layered Materials. *Nat. Nanotechnol.* **2013**, *8*, 952–958.

10. Fazio, D. D.; Goykhman, I.; Yoon, D.; Bruna, M.; Eiden, A.; Milana, S.; Sassi, U.; Barbone, M.; Dumcenco, D.; Marinov, K. *et al.* High Responsivity, Large-Area Graphene/MoS₂ Flexible Photodetectors. *ACS Nano* **2016**, *10*, 8252–8262.
11. Yu, W. J.; Vu, Q. A.; Oh, H.; Nam, H. G.; Zhou, H. L.; Cha, S.; Kim, J. Y.; Carvalho, A.; Jeong, M.; Choi, H. *et al.* Unusually Efficient Photocurrent Extraction in Monolayer van der Waals Heterostructure by Tunnelling through Discretized Barriers. *Nat. Commun.* **2016**, *7*, 13278.
12. Britnell, L.; Ribeiro, R. M.; Eckmann, A.; Jalil, R.; Belle, B. D.; Mishchenko, A.; Kim, Y.-J.; Gorbachev, R. V.; Georgiou, T.; Morozov, S. V. *et al.* Strong Light-Matter Interactions in Heterostructures of Atomically Thin Films. *Science* **2013**, *340*, 1311–1314.
13. Morozov, S. V.; Novoselov, K. S.; Katsnelson, M. I.; Schedin, F.; Elias, D. C.; Jaszczak, J. A.; Geim, A. K. Giant Intrinsic Carrier Mobilities in Graphene and Its Bilayer. *Phys. Rev. Lett.* **2008**, *100*, 016602.
14. Liu, H.-L.; Shen, C.-C.; Su, S.-H.; Hsu, C.-L.; Li, M.-Y.; Li, L.-J. Optical Properties of Monolayer Transition Metal Dichalcogenides Probed by Spectroscopic Ellipsometry. *Appl. Phys. Lett.* **2014**, *105*, 201905.
15. Chiu, M. H.; Zhang, C. D.; Shiu, H. W.; Chu, C. P.; Chen, C. H.; Chang, C. Y. S.; Chen, C. H.; Chou, M. Y.; Shih, C. K.; Li, L. J. Determination of Band Alignment in the Single-Layer MoS₂/WSe₂ Heterojunction. *Nat. Commun.* **2015**, *6*, 7666.
16. Fang, H.; Battaglia, C.; Carraro, C.; Nemsak, S.; Ozdol, B.; Kang, J. S.; Bechtel, H. A.; Desai, S. B.; Kronast, F.; Unal, A. A. *et al.* Strong Interlayer Coupling in van der Waals Heterostructures Built From Single-Layer Chalcogenides. *Proc. Natl. Acad. Sci. U. S. A.* **2014**, *111*, 6198–6202.

17. Hong, X.; Kim, J.; Shi, S. F.; Zhang, Y.; Jin, C.; Sun, Y.; Tongay, S.; Wu, J.; Zhang, Y.; Wang, F. Ultrafast Charge Transfer in Atomically Thin MoS₂/WS₂ Heterostructures. *Nat. Nanotechnol.* **2014**, *9*, 682–686.
18. Ceballos, F.; Bellus, M. Z.; Chiu, H. Y.; Zhao, H. Ultrafast Charge Separation and Indirect Exciton Formation in a MoS₂-MoSe₂ van der Waals Heterostructure. *ACS Nano* **2014**, *8*, 12717–12724.
19. Rivera, P.; Schaibley, J. R.; Jones, A. M.; Ross, J. S.; Wu, S.; Aivazian, G.; Klement, P.; Seyler, K.; Clark, G.; Ghimire, N. J. *et al.* Observation of Long-Lived Interlayer Excitons in Monolayer MoSe₂-WSe₂ Heterostructures. *Nat. Commun.* **2015**, *6*, 6242.
20. Lee, C. H.; Lee, G. H.; van der Zande, A. M.; Chen, W.; Li, Y.; Han, M.; Cui, X.; Arefe, G.; Nuckolls, C.; Heinz, T. F. *et al.* Atomically Thin P-N Junctions with van der Waals Heterointerfaces. *Nat. Nanotechnol.* **2014**, *9*, 676–681.
21. Rivera, P.; Seyler, K. L.; Yu, H. Y.; Schaibley, J. R.; Yan, J. Q.; Mandrus, D. G.; Yao, W.; Xu, X. D. Valley-Polarized Exciton Dynamics in a 2D Semiconductor Heterostructure. *Science* **2016**, *351*, 688–691.
22. Schaibley, J. R.; Rivera, P.; Yu, H. Y.; Seyler, K. L.; Yan, J. Q.; Mandrus, D. G.; Taniguchi, T.; Watanabe, K.; Yao, W.; Xu, X. D. Directional Interlayer Spin-Valley Transfer in Two-Dimensional Heterostructures. *Nat. Commun.* **7**, 13747.
23. Xu, W. G.; Liu, W. W.; Schmidt, J. F.; Zhao, W. J.; Lu, X.; Raab, T.; Diederichs, C.; Gao, W. B.; Seletskiy, D. V.; Xiong, Q. H. Correlated Fluorescence Blinking in Two-Dimensional Semiconductor Heterostructures. *Nature* **2017**, *541*, 62.
24. Sun, J.; Lee, H. W.; Pasta, M.; Yuan, H. T.; Zheng, G. Y.; Sun, Y. M.; Li, Y. Z.; Cui, Y. A Phosphorene-Graphene Hybrid Material as a High-Capacity Anode for Sodium-Ion Batteries. *Nat. Nanotechnol.* **2015**, *10*, 980.

25. Huang, M. Q.; Li, S. M.; Zhang, Z. F.; Xiong, X.; Li, X. F.; Wu, Y. Q. Multifunctional High-Performance Van Der Waals Heterostructures. *Nat. Nanotechnol.* **2017**, *12*, 1148.
26. Shim, J.; Oh, S.; Kang, D. H.; Jo, S. H.; Ali, M. H.; Choi, W. Y.; Heo, K.; Jeon, J.; Lee, S.; Kim, M. *et al.* Phosphorene/Rhenium Disulfide Heterojunction-Based Negative Differential Resistance Device for Multi-Valued Logic. *Nat. Commun.* **2016**, *7*, 13413.
27. Wang, F.; Wang, Z. X.; Xu, K.; Wang, F. M.; Wang, Q. S.; Huang, Y.; Yin, L.; He, J. Tunable GaTe-MoS₂ van Der Waals P-N Junctions with Novel Optoelectronic Performance. *Nano Lett.* **2015**, *15*, 7558–7566.
28. Vargas, A.; Liu, F. Z.; Lane, C.; Rubin, D.; Bilgin, I.; Hennighausen, Z.; DeCapua, M.; Bansil, A.; Kar, S. Tunable and Laser-Reconfigurable 2d Heterocrystals Obtained by Epitaxial Stacking of Crystallographically Incommensurate Bi₂Se₃ and MoS₂ Atomic Layers. *Sci. Adv.* **2017**, *3*, e1601741.
29. Zhong, D.; Seyler, K. L.; Linpeng, X. Y.; Cheng, R.; Sivadas, N.; Huang, B.; Schmidgall, E.; Taniguchi, T.; Watanabe, K.; McGuire, M. A. *et al.* Van Der Waals Engineering of Ferromagnetic Semiconductor Heterostructures for Spin and Valleytronics. *Sci. Adv.* **2017**, *3*, e1603113.
30. Niu, L.; Liu, X. F.; Cong, C. X.; Wu, C. Y.; Wu, D.; Chang, T. R.; Wang, H.; Zeng, Q. S.; Zhou, J. D.; Wang, X. L. *et al.* Controlled Synthesis of Organic/Inorganic Van Der Waals Solid for Tunable Light-Matter Interactions. *Adv. Mater.* **2015**, *27*, 7800–7808.
31. Cheng, H. C.; Wang, G. M.; Li, D. H.; He, Q. Y.; Yin, A. X.; Liu, Y.; Wu, H.; Ding, M. N.; Huang, Y.; Duan, X. F. Van Der Waals Heterojunction Devices Based on Organohalide Perovskites and Two-Dimensional Materials. *Nano Lett.* **2016**, *16*, 367–373.
32. Liu, X.; Gu, J.; Ding, K.; Fan, D. J.; Hu, X. E.; Tseng, Y. W.; Lee, Y. H.; Menon, V.; Forrest, S. R. Photoresponse of an Organic Semiconductor/Two-Dimensional Transition Metal Dichalcogenide Heterojunction. *Nano Lett.* **2017**, *17*, 3176–3181.

33. Huang, Y.; Zhuge, F. W.; Hou, J. X.; Lv, L.; Luo, P.; Zhou, N.; Gan, L.; Zhai, T. Y. Van Der Waals Coupled Organic Molecules with Monolayer MoS₂ for Fast Response Photodetectors with Gate-Tunable Responsivity. *ACS Nano* **2018**, *12*, 4062–4073.
34. Kafle, T.; Kattel, B.; Lane, S. D.; Wang, T.; Zhao, H.; Chan, W. L. Charge Transfer Exciton and Spin Flipping at Organic-Transition Metal Dichalcogenide Interfaces. *ACS Nano* **2017**, *11*, 10184–10192.
35. Shah, A.; Torres, P.; Tscharnner, R.; Wyrsh, N.; Keppner, H. Photovoltaic Technology: The Case for Thin-Film Solar Cells. *Science* **1999**, *285*, 692–698.
36. Lecomber, P. G.; Spear, W. E.; Ghaith, A. Amorphous-Silicon Field-Effect Device and Possible Application. *Electron. Lett.* **1979**, *15*, 179–181.
37. Nomura, K.; Ohta, H.; Takagi, A.; Kamiya, T.; Hirano, M.; Hosono, H. Room-Temperature Fabrication of Transparent Flexible Thin-Film Transistors Using Amorphous Oxide Semiconductors. *Nature* **2004**, *432*, 488–492.
38. Suslick, K. S.; Choe, S. B.; Cichowlas, A. A.; Grinstaff, M. W. Sonochemical Synthesis of Amorphous Iron. *Nature* **1991**, *353*, 414–416.
39. Smith, R. D. L.; Prevot, M. S.; Fagan, R. D.; Zhang, Z. P.; Sedach, P. A.; Siu, M. K. J.; Trudel, S.; Berlinguette, C. P. Photochemical Route for Accessing Amorphous Metal Oxide Materials for Water Oxidation Catalysis. *Science* **2013**, *340*, 60–63.
40. Yang, Z.; Hao, J.; Yuan, S.; Lin, S.; Yau, H. M.; Dai, J.; Lau, S. P. Field-Effect Transistors Based on Amorphous Black Phosphorus Ultrathin Films by Pulsed Laser Deposition. *Adv. Mater.* **2015**, *27*, 3748–3754.
41. Guo, Y. Z.; Robertson, J. Band Engineering in Transition Metal Dichalcogenides: Stacked Versus Lateral Heterostructures. *Appl. Phys. Lett.* **2016**, *108*, 233104.

42. Cai, Y.; Zhang, G.; Zhang, Y. W. Layer-Dependent Band Alignment and Work Function of Few-Layer Phosphorene. *Sci. Rep.* **2014**, *4*, 6677.
43. Ye, Z.; Cao, T.; O'Brien, K.; Zhu, H.; Yin, X.; Wang, Y.; Louie, S. G.; Zhang, X. Probing Excitonic Dark States in Single-Layer Tungsten Disulphide. *Nature* **2014**, *513*, 214–218.
44. Zhu, B.; Zeng, H.; Dai, J.; Gong, Z.; Cui, X. Anomalously Robust Valley Polarization and Valley Coherence in Bilayer WS₂. *Proc. Nat. Acad. Sci. USA* **2014**, *111*, 11606–11611.
45. Zhao, W. J.; Ghorannevis, Z.; Chu, L. Q.; Toh, M. L.; Kloc, C.; Tan, P. H.; Eda, G. Evolution of Electronic Structure in Atomically Thin Sheets of WS₂ and WSe₂. *ACS Nano* **2013**, *7*, 791–797.
46. Peimyoo, N.; Shang, J. Z.; Cong, C. X.; Shen, X. N.; Wu, X. Y.; Yeow, E. K. L.; Yu, T. Nonblinking, Intense Two-Dimensional Light Emitter: Mono Layer WS₂ Triangles. *ACS Nano* **2013**, *7*, 10985–10994.
47. Ceballos, F.; Cui, Q.; Bellus, M. Z.; Zhao, H. Exciton Formation in Monolayer Transition Metal Dichalcogenides. *Nanoscale* **2016**, *8*, 11681–11688.
48. Mai, C.; Semenov, Y. G.; Barrette, A.; Yu, Y. F.; Jin, Z. H.; Cao, L. Y.; Kim, K. W.; Gundogdu, K. Exciton Valley Relaxation in a Single Layer of WS₂ Measured by Ultrafast Spectroscopy. *Phys. Rev. B* **2014**, *90*, 041414.
49. He, J.; He, D.; Wang, Y.; Cui, Q.; Ceballos, F.; Zhao, H. Spatiotemporal Dynamics of Excitons in Monolayer and Bulk WS₂. *Nanoscale* **2015**, *7*, 9526.
50. Bellus, M. Z.; Yang, Z. B.; Hao, J. H.; Lau, S. P.; Zhao, H. Amorphous Two-Dimensional Black Phosphorus with Exceptional Photocarrier Transport Properties. *2D Mater.* **2017**, *4*, 025063.
51. Hoebe, F. J. M.; Jonkheijm, P.; Meijer, E. W.; Schenning, A. About Supramolecular Assemblies of Pi-Conjugated Systems. *Chem. Rev.* **2005**, *105*, 1491–1546.

52. Dexter, D. L. A Theory of Sensitized Luminescence in Solids. *J. Chem. Phys.* **1953**, *21*, 836–850.
53. Murphy, C. B.; Zhang, Y.; Troxler, T.; Ferry, V.; Martin, J. J.; Jones, W. E. Probing Förster and Dexter Energy-Transfer Mechanisms in Fluorescent Conjugated Polymer Chemosensors. *J. Phys. Chem. B* **2004**, *108*, 1537–1543.
54. Ceballos, F.; Bellus, M. Z.; Chiu, H. Y.; Zhao, H. Probing Charge Transfer Excitons in a MoSe₂-WS₂ van der Waals Heterostructure. *Nanoscale* **2015**, *7*, 17523–17528.
55. Peng, B.; Yu, G.; Liu, X.; Liu, B.; Liang, X.; Bi, L.; Deng, L.; Sum, T. C.; Loh, K. P. Ultrafast Charge Transfer in MoS₂/WSe₂ P-N Heterojunction. *2D Mater.* **2016**, *3*, 025020.
56. Zhu, H. M.; Wang, J.; Gong, Z. Z.; Kim, Y. D.; Hone, J.; Zhu, X. Y. Interfacial Charge Transfer Circumventing Momentum Mismatch at Two-Dimensional Van Der Waals Heterojunctions. *Nano Lett.* **2017**, *17*, 3591–3598.
57. Haigh, S. J.; Gholinia, A.; Jalil, R.; Romani, S.; Britnell, L.; Elias, D. C.; Novoselov, K. S.; Ponomarenko, L. A.; Geim, A. K.; Gorbachev, R. Cross-Sectional Imaging of Individual Layers and Buried Interfaces of Graphene-Based Heterostructures and Superlattices. *Nat. Mater.* **2012**, *11*, 764–767.
58. Golla, D.; Chattrakun, K.; Watanabe, K.; Taniguchi, T.; LeRoy, B. J.; Sandhu, A. Optical thickness determination of hexagonal boron nitride flakes. *Appl. Phys. Lett.* **2013**, *102*, 161906.
59. V., G. R.; Ibtisam, R.; R., N. R.; Rashid, J.; Liam, B.; D., B. B.; W., H. E.; S., N. K.; Kenji, W.; Takashi, T. *et al.* Hunting for Monolayer Boron Nitride: Optical and Raman Signatures. *Small* *7*, 465–468.
60. Bellus, M. Z.; Ceballos, F.; Chiu, H.-Y.; Zhao, H. Tightly Bound Trions in Transition Metal Dichalcogenide Heterostructures. *ACS Nano* **2015**, *9*, 6459–6464.

61. Boulesbaa, A.; Huang, B.; Wang, K.; Lin, M. W.; Mahjouri-Samani, M.; Rouleau, C.; Xiao, K.; Yoon, M.; Sumpter, B.; Puretzky, A. *et al.* Observation of Two Distinct Negative Trions in Tungsten Disulfide Monolayers. *Phys. Rev. B* **2015**, *92*, 115443.

Graphical TOC Entry

